Analysis of the longitudinal stability of a bioinspired morphing UAV

Rafael Bardera Mora
Javier Muñoz-Campillejo
Estela Barroso Barderas
Juan Carlos Matías García

Experimental Aerodynamics
Instituto Nacional de Técnica Aeroespacial (INTA)
Torrejón de Ardoz, Madrid
SPAIN

barderar@inta.es

ABSTRACT

The inherent characteristics of Unmanned Aerial Vehicles (UAVs) allow for the development of novel and innovative designs, usually implementing state-of-the-art technology, without having to deal with the number of restrictions associated with the development of bigger vehicles, specifically in terms of ensuring said vehicles are granted their certification. Moreover, the development of UAVs has significantly lower costs, which is particularly true of Micro Aerial Vehicles (MAVs). Consequently, during the last few years, the Instituto Nacional de Técnica Aeroespacial "Esteban Terradas" (INTA) has been developing a brand-new bioinspired UAV based on morphing wing technology with a Zimmerman planform using Macro Fiber Composite (MFC) actuators. With the project still being in an early development stage, ensuring the stability of the drone is paramount, especially given its geometrical configuration. In order to achieve said stability, a T-tail configuration was chosen. While a preliminary longitudinal stability analysis of the base configuration of the bioinspired morphing UAV has already been conducted by means of a Stability Augmentation System (SAS) together with a PID-based pitch autopilot, the influence of modifying the wing with the MFC actuator on the longitudinal stability remain to be assessed. Therefore, in the present work, an analysis of the longitudinal stability of the considered bioinspired morphing UAV with a modified configuration will be undertaken and compared with that of the base configuration. An assessment of whether or not the modification of the PID coefficients prove to be beneficial will also be made.

1.0 INTRODUCTION

An aircraft with a morphing wing can be defined as one with the ability to deform its own wing geometry in-flight in order to optimize its aerodynamic performance [1]. This type of vehicle is not new at all, since aircrafts with adaptive wing geometry have been developed throughout history, going back to the Wright brothers, who applied structural deformations to change the aerodynamic characteristics [2]. Later on, the Bell X5 was the first aircraft capable of changing the wing deflection in-flight. The technology behind is however significantly different to that used nowadays, and currently, the design of morphing manned aircrafts is restricted in terms of actuators and flexible structures. However, the implementation of bioinspired solutions in Unmanned Aerial Vehicles (UAVs) has been undergoing a rapid evolution during the last years, and as such it has been the main object of numerous studies, as seen in Refs. [3 – 6]. Morphing wing technology allows for the optimization of the aerodynamic characteristics according to each specific flight segment, thus also adapting its range and autonomy to the mission requirements. In addition, this technology can be implemented by means of innovative wing-integrated devices, which reduce or get rid of the aerodynamic discontinuities of conventional control surfaces such as flaps or elevator, while also reducing the weight of the necessary mechanisms.

There is a wide variety of morphing wing solutions depending on the specific wing parameter that undergoes a modification. In Ref. [1], a widely used classification is proposed: planform deformation (wingspan, chord or sweep angle will be the modified parameters), out-of-plane transformation (bending or twisting) and airfoil profile adjustment. An example of this technology is the morphing demonstrator developed in Ref. [7] to analyze the effects of gull-wings on a typical flight of a small Remotely Piloted Air Vehicle (RPAS). In addition to modifying the aerodynamic performance, the vehicle's stability and its dynamic modes we also affected by the wing deformation. In Ref. [8], the implementation of several independent wing control surfaces in place of conventional ailerons was studied to both control the roll mode and complement other control surfaces such as the elevator, the rudder and the flaps, which improved pitch, roll and yaw responses and minimized the induced drag. A control system based on a pair of winglets with adaptative cant angle was also studied in the work of Ref. [9] with independent actuators, which resulted in a beneficial coupling of the pitch and roll of the aircraft. Another example is the development of a trailing edge morphing mechanism by means of Macro Fiber Composite (MFC) actuators implemented in a typical MAV, as shown in Ref. [10], resulting in an increase in lift to drag ratio as compared with conventional wings.

In the present work, the implementation of MFC actuators in order to achieve an adaptative wing geometry capable of modifying its own camber in a bioinspired UAV with a Zimmerman planform and its effects on the vehicle's longitudinal stability are studied. On account of the wing's inherent characteristics, the vehicle resembles a flying wing aircraft and will thus be statically unstable. The implementation of angle of attack stability augmentation system (SAS) together with a pitch rate SAS [11] is therefore needed to achieve both a statically stable drone and a proper handling and system response against perturbations. Moreover, in order to further enhance the vehicle's stability and response, while making it capable of autonomous flight, a pitch angle autopilot is needed, which is usually implemented based on proportional-integral-derivative (PID) controllers [12 – 16], but alternative control laws can also be used [17, 18]. Since the increase in the wing camber proved to be incapable of making the vehicle statically stable, a typical T-tail configuration was chosen for its empennage. Given that PID controllers have been widely used for the aircraft pitch control [19 – 21] and have long been well-known [22, 23], an integrated pitch stability augmentation system with a PID-based autopilot was studied and designed in previous works to provide an adequate response against an elevator deflection perturbation. The gains of both the SAS and the autopilot were obtained with an iterative process using criteria such as the quality of the time response (settling time or overshoot) or the system's gain and phase stability margins, given the enormous uncertainties of the system and the great impact the actuators and sensors characteristic time-delays had on the stability. All the necessary transfer functions were obtained by means of the linearized equation of motion used to model the drone flight dynamics [24, 25]. However, the effects of modifying the wing's camber with the MFC actuator on the longitudinal stability and the integrated autopilot remained to be studied, and will thus be the main focus of the present work. Consequently, an assessment of whether or not the increase in camber is significant for the system's stability, or if the selected PID gains can be refined to further improve its response, will therefore be made.

1.1 Design of the bioinspired morphing UAV

The conceptual design of the considered bioinspired UAV considered in this work was developed by Ref [26], and its 3D CAD model is shown in Figure 1-1. Its main characteristic is the use of piezoceramic MFC (Macro Fiber Composite) actuators implemented within the wing and over the intrados surface to modify the airfoil curvature in-flight in order to optimize the drone's configuration to the specific requirement of each flight segment. A double goal is pursued with this modification. On the one hand, and increase in aerodynamic performance or efficiency is achieved with a lower curvature, thus leading to increased range and autonomy, making it the ideal configuration for the cruise phase. On the other hand, an increase in the maximum lift coefficient is obtained for a higher curvature, thus allowing the vehicle to fly at lower velocities without reaching stall conditions, i.e., to increase the stall speed, which could improve its real-time video recording characteristics, were that to be its mission, or simply improve its maneuverability and performance during landing and take-off phases.

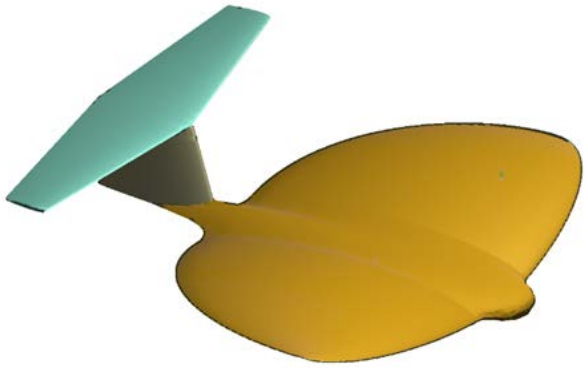

Figure 1-1: 3D CAD model of the bioinspired morphing UAV.

The wing and fuselage are composed of Eppler 61 and Whitcomb II airfoils, as shown in Figure 1-2, respectively. The Eppler 61 airfoil has been chosen due to several requirements. First of all, on account of the MFC actuators having to be placed over a convex intrados for them to be able to modify the wing curvature, the number of potential airfoils is greatly reduced since the intrados curvature of a great number of them is negative. Moreover, the airfoil needs to perform efficiently at low Reynolds numbers, preferably with a progressive stall entry. Given the ratio $\left(t/c\right)_{\max}$ of 5.64% of the Eppler 61 airfoil and its negative intrados curvature, both of these requirements are met. The Whitcomb II, however, was chosen for the fuselage merely for structural reasons so as to allow all the necessary UAV components to be integrated within said structure. What makes this UAV rather unique is its Zimmerman planform, which was selected because of its high aerodynamic performance, only surpassed by the elliptical planform, and is composed of two half-ellipses as seen in Figure 1-2.

On the other hand, the considered T-tail empennage is composed of a vertical and trapezoidal horizontal stabilizer with conventional NACA 0012 airfoils.

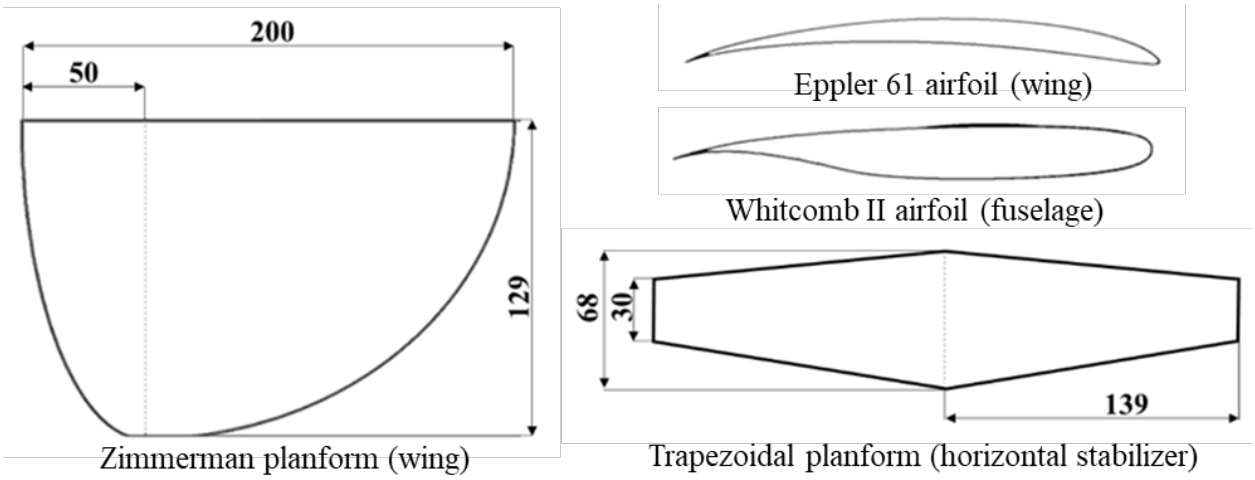

Figure 1-2: 3D Sketch of the main geometrical features of the morphing UAV (dimensions in mm).

Since the piezoelectric MFC actuators have a working range from 0V to 1500V, the base configuration of the morphing UAV will be composed of Eppler 61 airfoils only when the voltage input is 0V, and the forced applied by the actuators is thus zero. As the voltage applied to the actuators increases, the curvature of the

Eppler 61 airfoils begins to increase as well, until the maximum wing deformation is obtained at 1500V (see Figure 1-3). The increase of said curvature is not exactly linear with the voltage input, and the mathematics expressions have already been obtained in Refs. [26, 27]. In the figure below, some of the results achieved in Ref. [27] are shown:

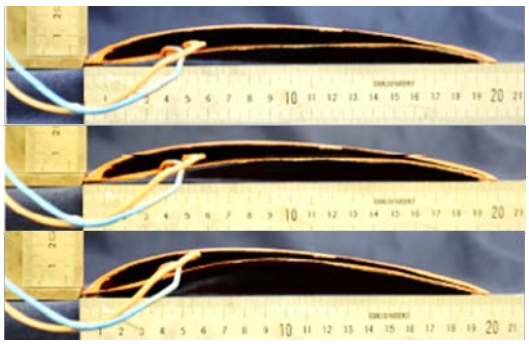

Airfoil curvature with 500 V.

Airfoil curvature with 1000 V.

Airfoil curvature with 1500 V (maximum wing deformation).

Figure 1-3: Deformation of the wing airfoils curvature for different voltage inputs.

Although the change in the airfoil curvature was only observed in the wing root (see Figure 1-3), said increase can be taken, as a first approximation, as constant throughout the whole wingspan, and therefore extrapolated to each section. Doing so results in the modified configuration of the bioinspired morphing UAV shown in Figure 1-4 besides its base configuration so as to visually compare both of them.

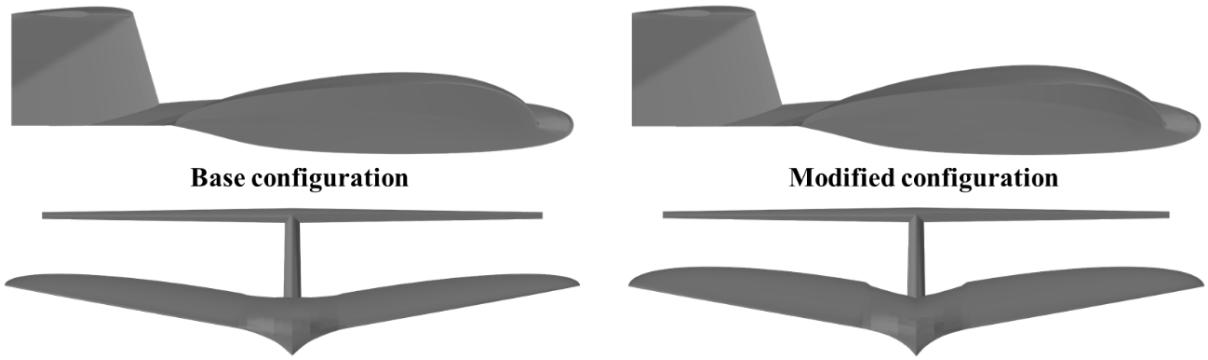

Figure 1-4: Comparison between the base and modified configurations of the morphing UAV.

Table 1-1: Overview of some geometrical features of the morphing UAV.

Geometrical Features	Value	Geometrical Features	Value
Reference wing surface, S_{ref}	40.000 mm^2	**Mean aerodynamic chord, MAC**	141 mm
Fuselage length, l	300 mm	**Mean geometry chord, MGC**	127 mm
Fuselage width, d	60 mm	**Taper ratio, λ**	0.124
Wingspan, b	320 mm	**Aspect ratio, AR**	2.500
Wing tip chord, c_t	25 mm	**Dihedral angle, D_h**	10°

2.0 LONGITUDINAL STABILITY ANALYSIS OF THE BASE AND MODIFIED CONFIGURATION

Having briefly explained the design of the considered bioinspired morphing UAV and having introduced both the base and the modified configuration, an analysis of the difference in the longitudinal stability between said configurations will be conducted in this section. First of all, the main stability derivative of the vehicle's longitudinal static stability is the pitching moment coefficient with respect to the angle of attack, or c_{m_α}, which can be obtained as shown in Eq. 1 and which will determine whether or not the drone is statically stable or unstable: if $c_{m_\alpha} < 0$ the vehicle will be statically stable, otherwise it will be statically unstable, since for a positive angle of attack perturbation, the response of the vehicle must be such that it counteracts said perturbation, reducing the angle of attack instead of incrementing it.

$$c_{m_\alpha} = \frac{\partial c_m}{\partial \alpha} = c_{L_\alpha}(\hat{x}_{cg} - \hat{x}_{ac}) \tag{1}$$

As c_{L_α} is the slope of the lift coefficient versus angle of attack curve, such as $c_L = c_{L_\alpha} \cdot \alpha$, it will therefore be always positive for airfoils with positive camber. Since $\hat{x}_{ac}$ and $\hat{x}_{cg}$ are the dimensionless longitudinal position of aerodynamic center and the center of mass, respectively, whether or not the c_{m_α} coefficient is positive or negative will ultimately come down just to the relative position between aerodynamic and gravity centers. It seems rather unlikely, therefore, that a change in the wing's curvature significantly affects its static stability.

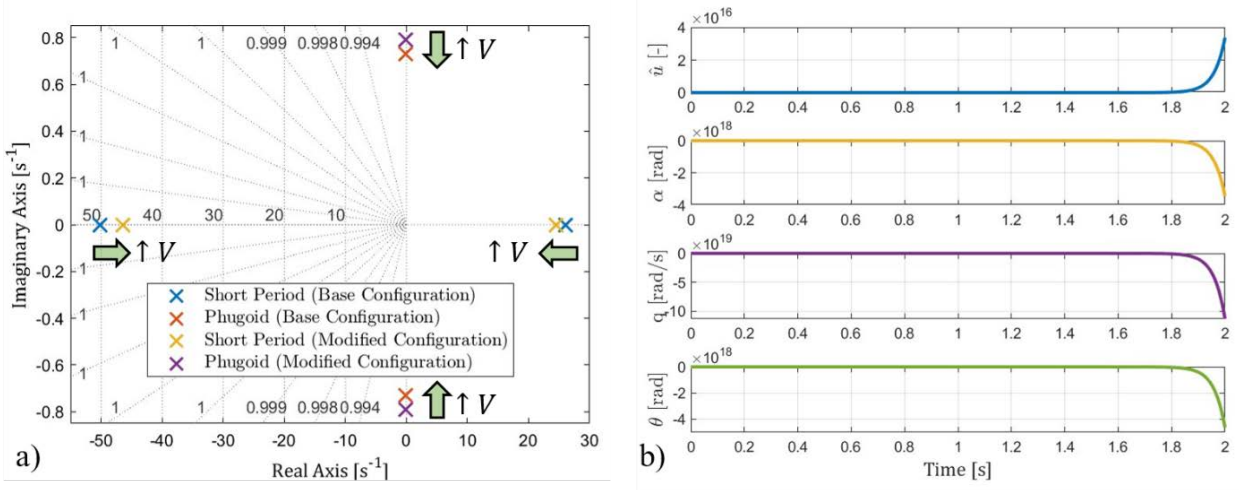

Figure 2-1: a) Longitudinal dynamic modes poles of both the morphing base and modified configurations. b) Time response of the latter's state variables for a given elevator deflection input.

To obtain an approximate value for the necessary stability derivatives to undertake the longitudinal stability analysis, an aerodynamic simulation has been run by means of XLFR5 software for both the base, which was already analyzed in previous works, and modified configurations. Since the aim of this analysis is not to be fully accurate but rather serve as a guide of whether or not the morphing UAV can be properly controlled as it stands and to compare both configurations, several simplifications were assumed. Specifically, thin airfoil surface and very small angles hypothesis were considered along with the incompressible and irrotational fluid hypothesis, and given that viscosity conditions could not be studied due to stall conditions, it was instead verified that the obtained trim conditions were far enough from said phenomenon, namely that $\alpha_{trim} \ll \alpha_{stall}$. Because of its higher accuracy, the Vortex Lattice Method or VLM was used in place of 3D panel method, and the Reynolds range considered was of $Re \in [3500 - 395000]$, with a Mach number of about $M = 0.03$ and an angle of attack range of $\alpha \in [-20°, 30°]$.

As expected, the static stability parameter of the modified configuration, $c_{m_\alpha}^{modified} = 0.67567\ \text{rad}^{-1} > 0$, did not differ much from the one obtained for the base configuration, $c_{m_\alpha}^{base} = 0.65744\ \text{rad}^{-1} > 0$, both of them being positive and thus implying the vehicle is statically unstable. Consequently, one or both longitudinal dynamic modes will be unstable, as is the case of the short period mode in particular, as shown in Figure 2-1 a, since one of the system's poles is located in the real right semiplane. As said pole is particularly located in the real axis as well, the short period will therefore be exponentially unstable, as can be seen in Figure 2-1 b, where the time response of every considered longitudinal state variables has been plotted against a certain elevator deflection input. The considered state variables are, in order, the pitch angle, θ, the angle of attack, α, the pitch rate, q, and the dimensionless velocity, $\hat{u}$.

Since not only is the pitch angle time response exponentially unstable, but also inverted, a longitudinal flight control system is mandatory, which will be explained in the next section.

3.0 REDESIGN OF THE FLIGHT CONTROL SYSTEM FOR THE MODIFIED CONFIGURATION

As has already been stated, a flight control system has been previously designed for the base configuration of the bioinspired morphing UAV by means of an integrated stability augmentation system (of both angle of attack and pitch rate) and a PID-based pitch angle autopilot, whose simplified diagram is shown in Figure 3-1 as reference.

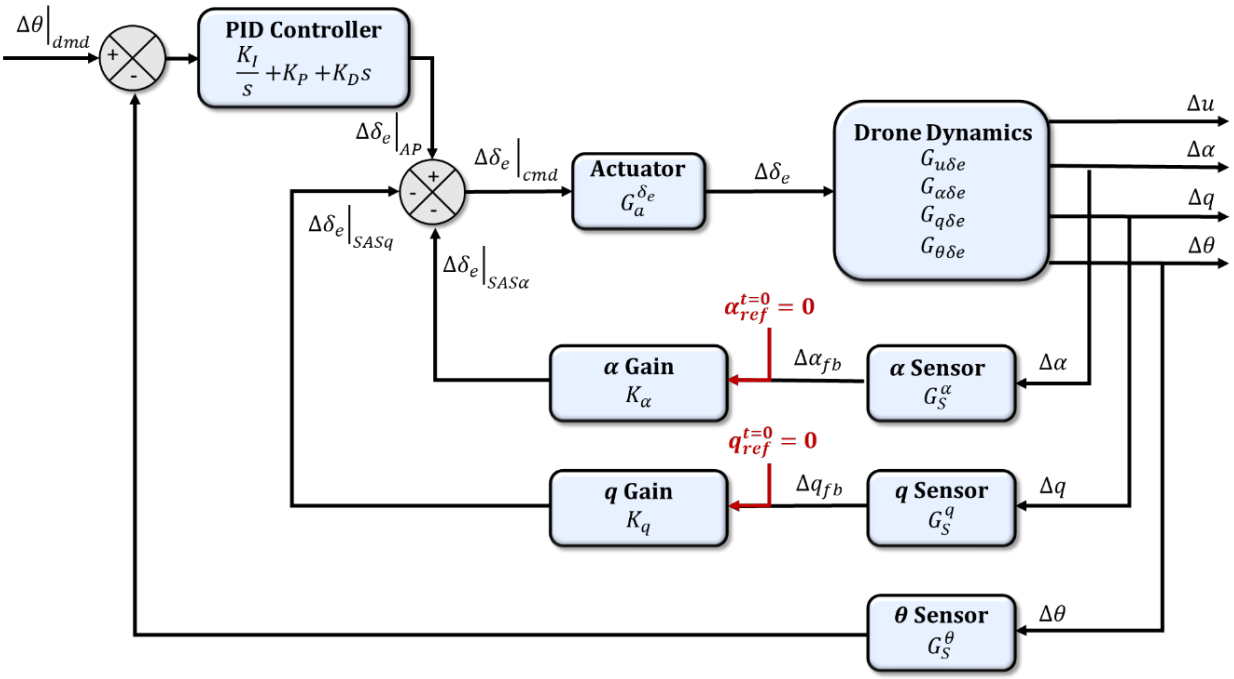

Figure 3-1: Diagram of the PID-based pitch angle autopilot with an integrated stability augmentation system

Aside from the drone dynamics transfer functions, which are obtained from the linearized equations of motion (see Refs. [24, 25]), the sensors and actuator involved in the flight control system were modeled as second order transfer functions as shown in Eq. 2 and Eq. 3 respectively, with the formers following a Padé approximation, as shown in

$$G_a^{\delta e} = \frac{w_a^2}{s^2 + 2\xi_a w_a s + 2w_a^2} \quad (2)$$

Where $\xi_a = 0.8$ is the damping coefficient, and w_a is the characteristic frequency of the actuator, $w_a = 1/\tau_a$, with $\tau_a = 0.01$ s being the response delay.

$$G_s = \frac{s^2 - 2w_s s + 2w_s^2}{s^2 + 2w_s s + 2w_s^2} \quad (3)$$

Where now no damping coefficients are involved and the characteristic frequency will instead be $w_s = 2/\tau_s$, with $\tau_s = 0.005$ s being the sensors characteristic response delay. All values have been taken so as to assume a more realistic model.

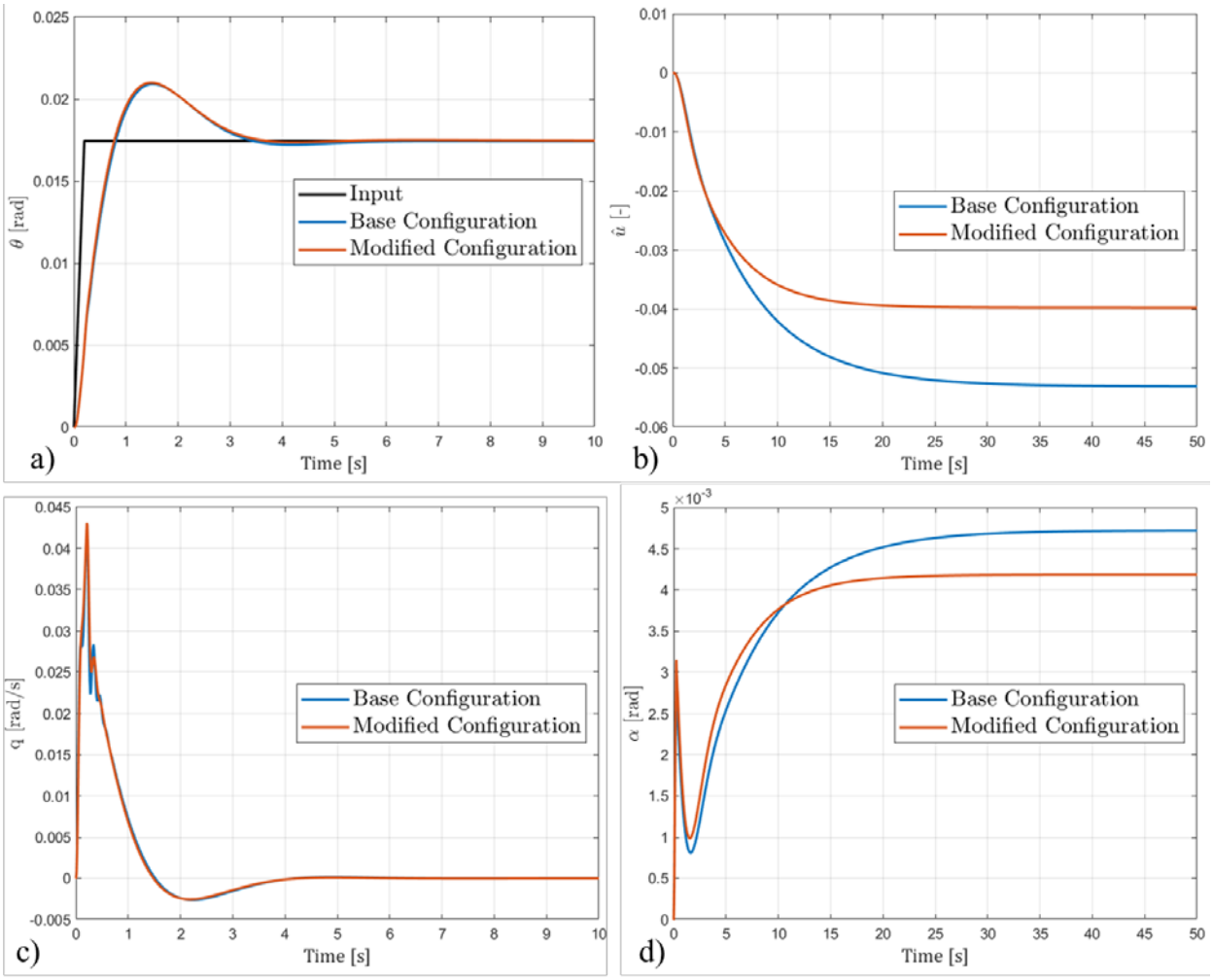

Figure 3-2: Comparison between the a) pitch angle, b) dimensionless velocity, c) pitch rate and d) angle of attack time responses for an input elevator deflection for the base and modified configurations using the same flight control system gains for both.

The flight control system gains obtained in that work to properly stabilize the base configuration of the morphing UAV are presented in Table 3-1 below.

Table 3-1: Flight control system gains previously obtained for the morphing base configuration

K_α	K_q	K_P	K_I	K_D
-1.375	-0.05	-0.15	-0.18	-0.004

Although the same gains obtained for the base configuration could be used for the modified configuration as well, no tangible benefit of the slight increase in the longitudinal stability shown in Figure 2-1 a would be achieved, since the pitch angle and pitch rate time responses against a perturbation of the elevator deflection remains virtually the same (see Figure 3-2 a and Figure 3-2 c, respectively). It should be noted however that both the stationary values of the dimensionless velocity and angle of attack time responses do differ significantly when comparing the modified and base configurations, albeit not because of the flight control system but because of the change in other stability derivatives consequence of the geometrical modification.

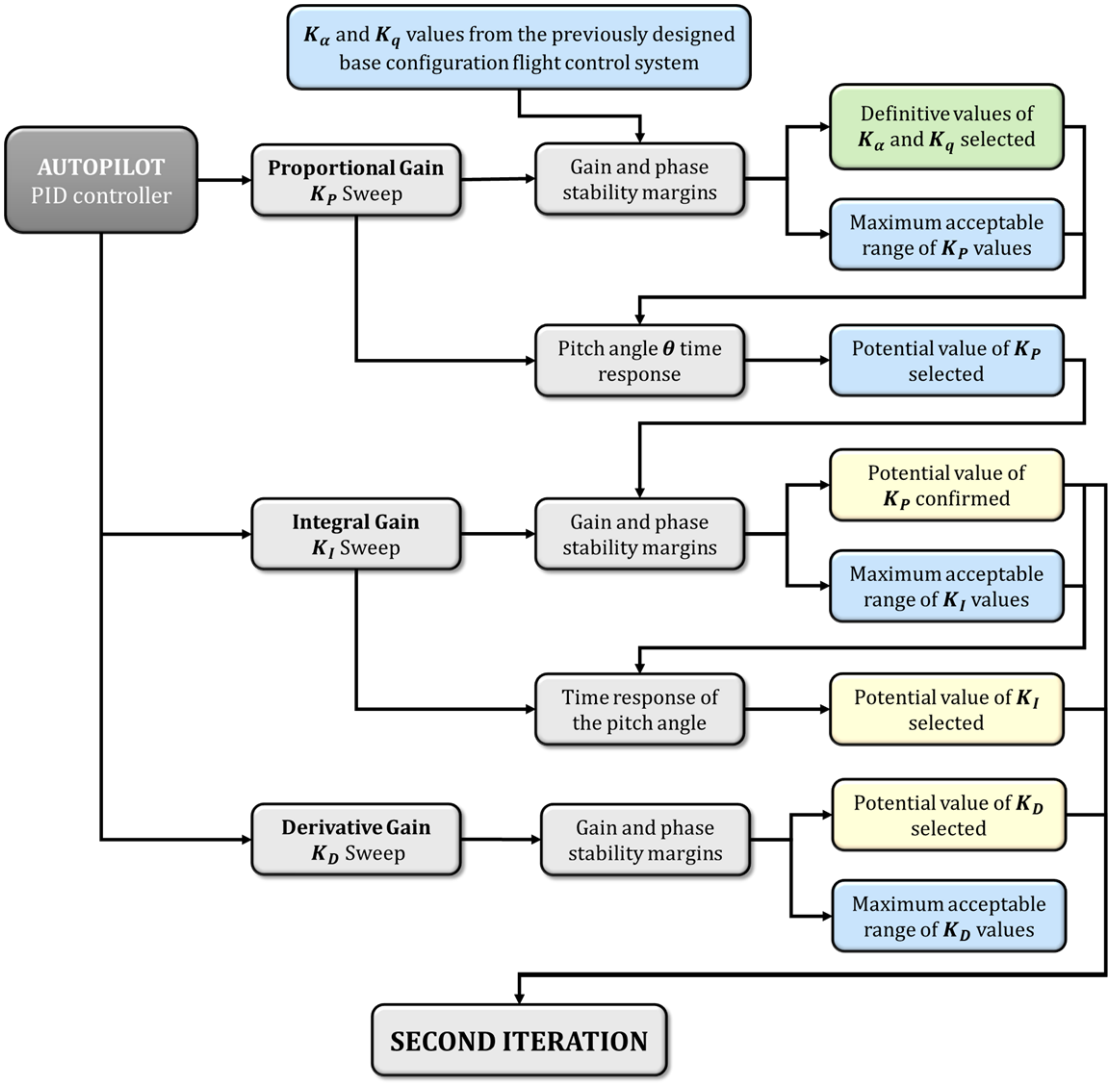

Figure 3-3: Simplified flow diagram of the first iteration of the flight control system redesign

Consequently, it could prove to be rather beneficial to redesign the flight control system gains, particularly the autopilot, so as to make better use of the stability improvement of the modified configuration. Doing so will

require two iterations, given the iterative nature of this process on account of the heavy influence of each gain over the others in terms of stability. Although different criteria could be used, in the present work the SAS and autopilot gains are going to selected by means of the gain and phase stability margins and the quality of the pitch angle time response, both in terms of the system's settling time and its overshoot. The minimum acceptable values for gain and phase margin will be $GM_{\min} = 6$ dB and $PM_{\min} = 45°$. In Figure 3-3, a simplified flow diagram of the first iteration is presented.

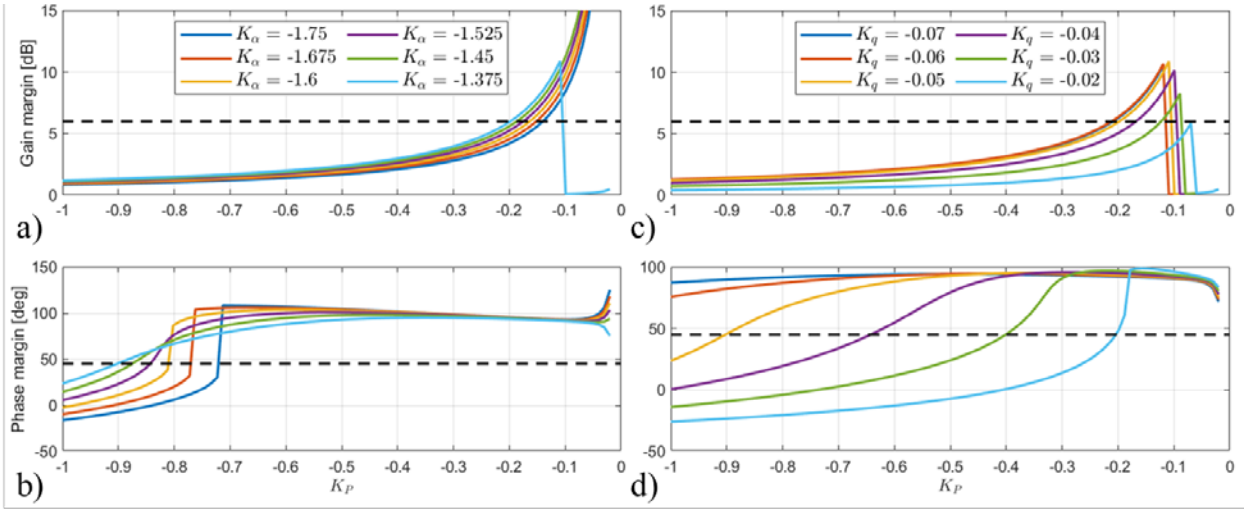

Figure 3-4: Evolution with K_P of the modified configuration's a) gain and b) phase margins for different K_α values for $K_q = -0.05$ and c) gain and d) phase margins for different K_q values for a given $K_\alpha = -1.375$

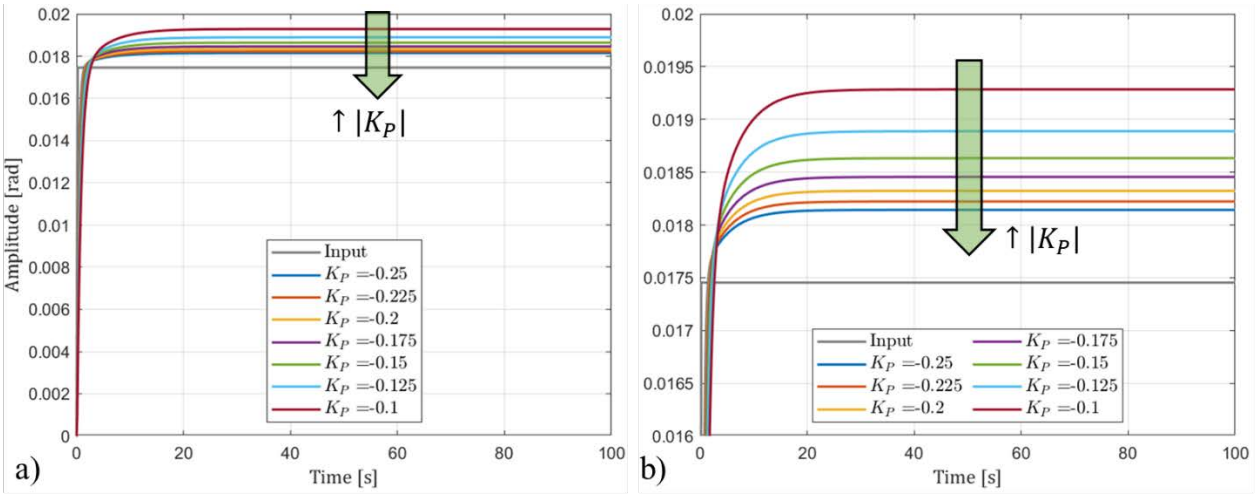

Figure 3.5: a) Pitch angle time response for a given elevator deflection perturbation with the selected SAS gains for different values of K_P and b) said time response in detail.

The first step of the redesign will thus be to check whether the SAS gains, K_α and K_q need to be modified or not. However, as presented in Figure 3-4, where the evolution of the gain and phase stability margins with the proportional gain K_P have been obtained for different values of K_α and K_q (taking the other one as constant), the base configuration values of $K_\alpha = -1.375$ and $K_q = -0.05$ are still good enough for the modified configuration, although the latter could be slightly modified from -0.05 to $K_q = -0.06$ to further increase

the range of acceptable K_P values. In this particular case, the limiting requirement will be the gain margin, since for $K_P < -0.2$ the value of GM_{min} is not met.

Observing the pitch angle time response for a given elevator deflection perturbation using the selected gains of $K_\alpha = -1.375$ and $K_q = -0.06$ (see Figure 3-5), it becomes clear that higher values of $|K_P|$, limited by the gain margin, would be desirable so as to minimize the stationary error and slightly reduce the rise time, thus improving the system's response.

Although a value of $K_P = -0.2$ seems optimal, the effects of including a non-zero integral gain on the stability margins must be assessed. As can be seen in Figure 3-6, however, while slightly decreasing as $|K_I|$ increases, the gain margin remains roughly constant for a given K_P. In addition, it can be clearly observed that an increase in $|K_P|$ benefits the phase margin, but negatively affects the gain margin.

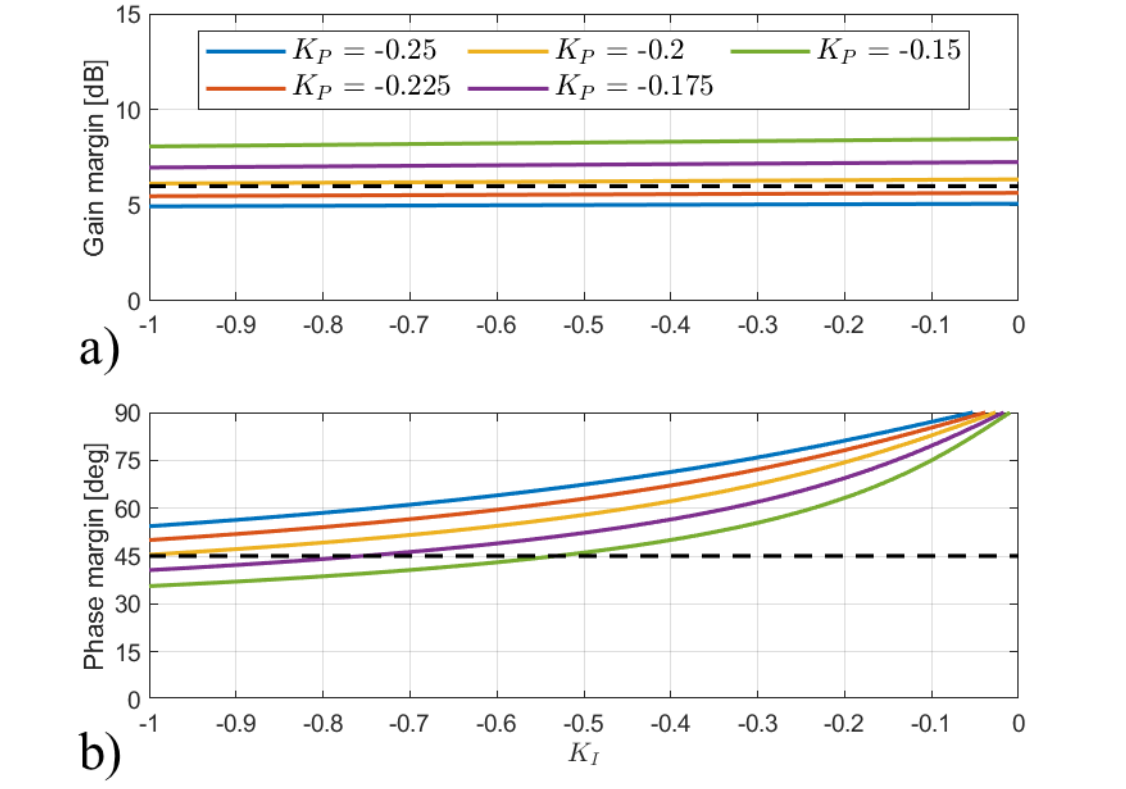

Figure 3-6: Evolution with K_I of the modified configuration's a) gain and b) phase margins for different K_P values for the selected SAS gains

Therefore, if $K_P = -0.2$ is taken as temporary value, virtually any value of K_I could be chosen. To properly select a potential integral gain, the pitch angle time response, presented in Figure 3-7, is needed. In this case, no immediate conclusion may be extracted, since while increasing $|K_I|$ reduces the settling time, the response becomes under-dampened, and the overshoot significantly increases. Selecting a value of $K_I \approx -0.5$ could therefore be optimal, with the restricting factor mostly being the overshoot.

In order to confirm the selection of this integral gain, its effects on the stability margins when derivative gains are included must be studied as well. However, only very small values of $|K_D|$ may be considered on account of the gain margin quickly going below the GM_{min} requirement for higher values. Although the gain margin

values do not differ much for different integral gains, higher values of $|K_I|$ do have a negative effect in the phase margin, albeit always meeting the PM_{min} requirement for the considered range. Therefore, an integral gain of $K_I = -0.05$ can be used. The most interesting characteristic of Figure 3-8 a is, however, the relatively steep increase in gain margin for a derivative gain as small as $K_D \approx -0.004$, going from about 6 dB to almost 8 dB.

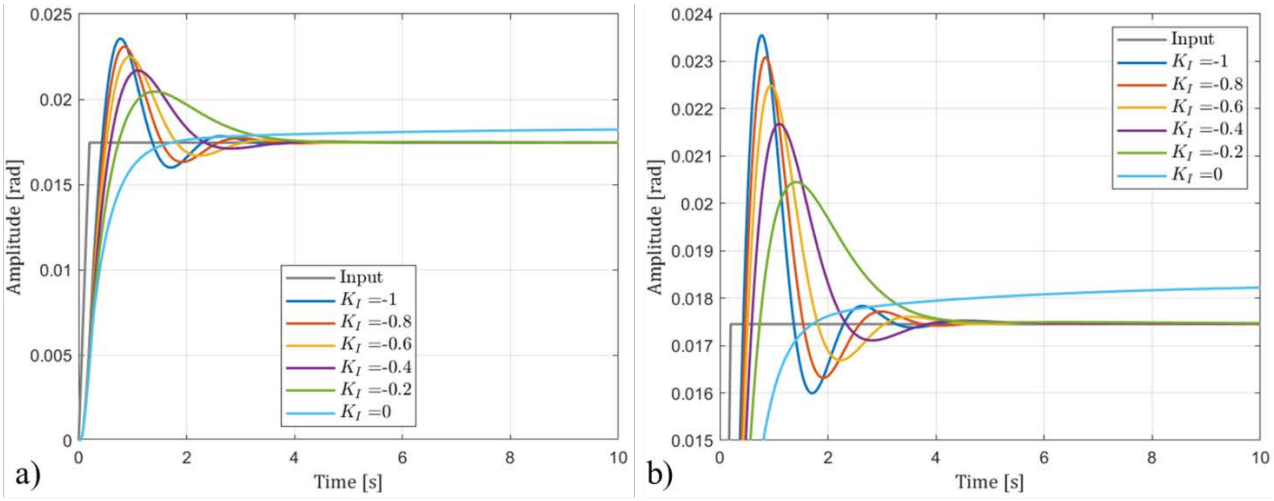

Figure 3-7: a) Pitch angle time response for a given elevator deflection perturbation with the selected SAS and proportional gains for different values of K_I and b) said time response in detail.

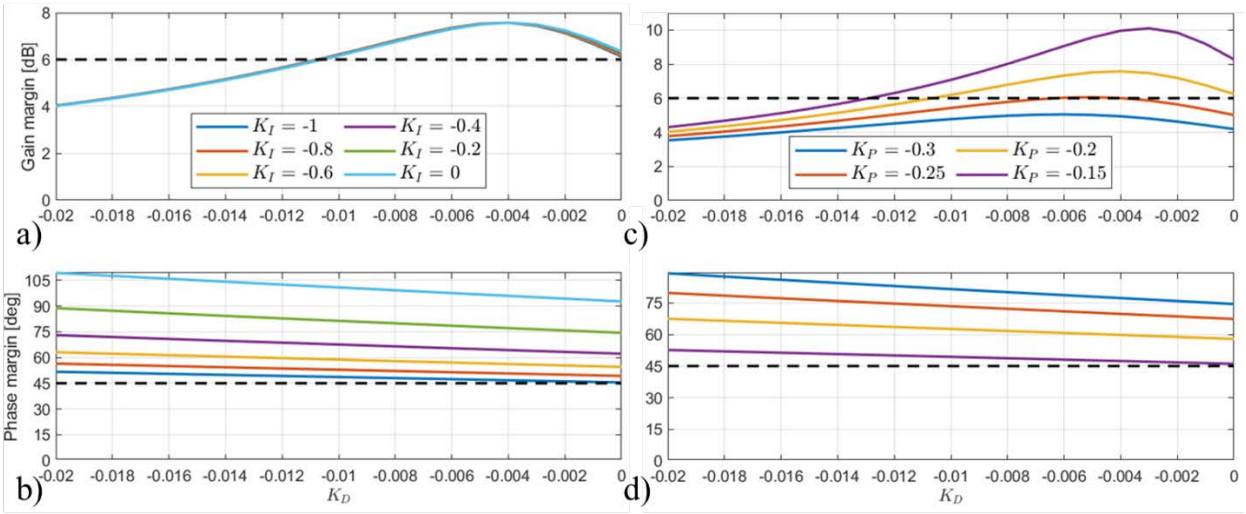

Figure 3-8: Evolution with K_D of the modified configuration's a) gain and b) phase margins for different K_I values for $K_P = -0.2$ and c) gain and d) phase margins for different K_P values for $K_I = -0.5$

The main consequence of this phenomenon is that the proportional gain may now be further increased while still complying with the gain and phase margin requirements, as presented in Figure 3-8 b, with the added benefit that higher values of $|K_P|$ will increase the phase margin as well, so that the effect of increasing $|K_I|$ is countered. Hence, the importance of adding a second iteration to the flight control system design process, whose simplified flow diagram is shown in Figure 3-9 below, now that potential or provisional values of each considered gain have been selected, and that the effects of increasing or reducing each one of them are known.

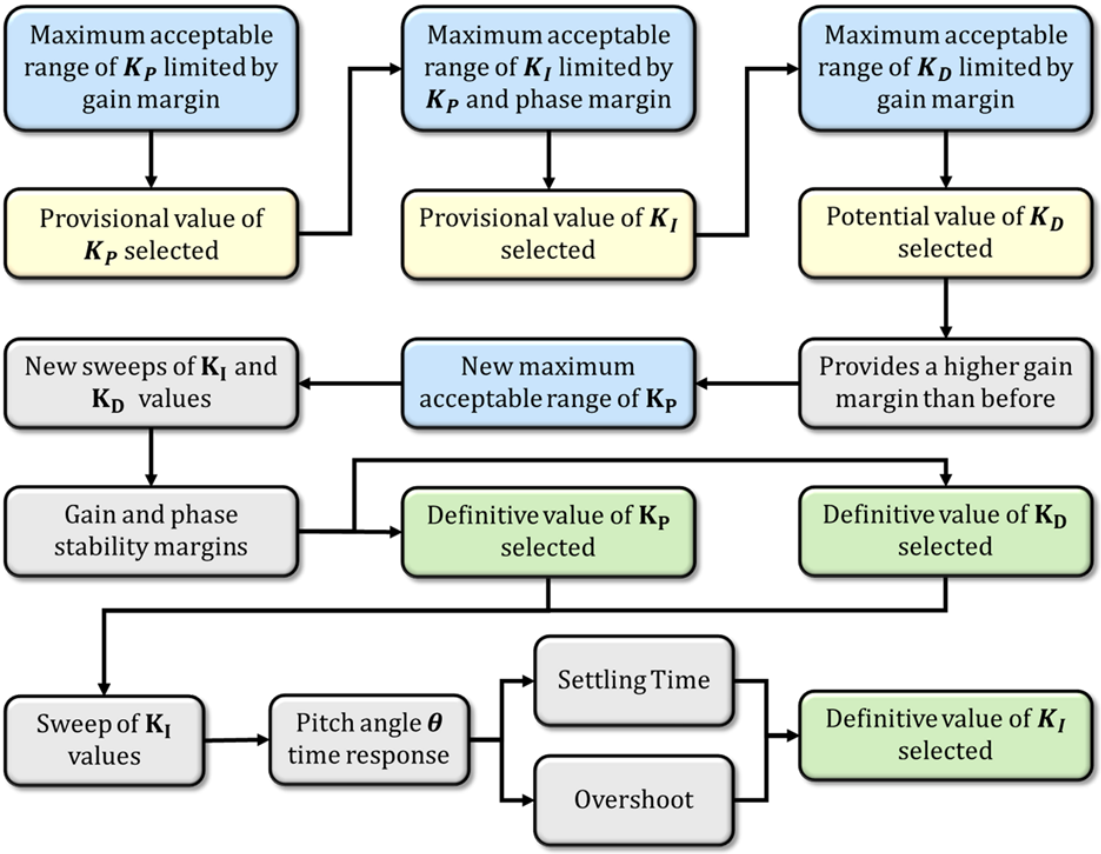

Figure 3-9: Simplified flow diagram of the second iteration of the flight control system redesign

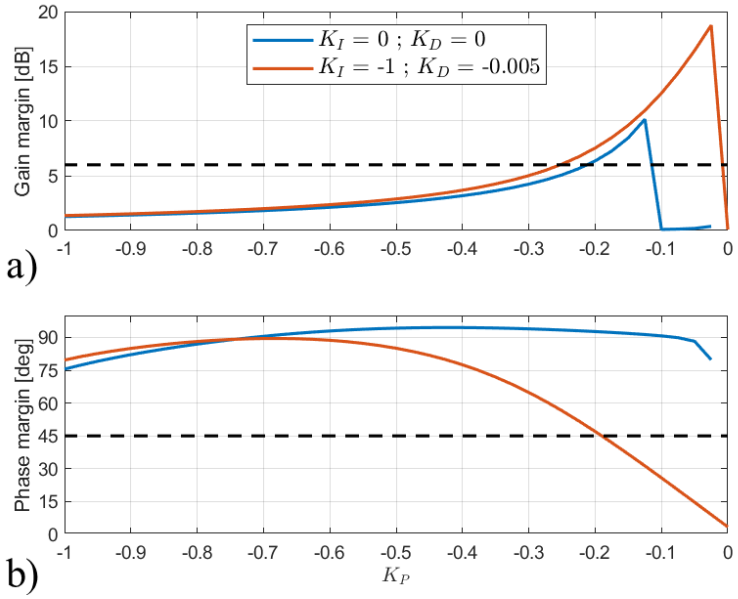

Figure 3-10: Evolution with of the modified configuration's a) gain and b) phase margins before and after considering the potential integral and derivative gains from the first iteration

As can be seen in Figure 3-8 b, the value of $|K_D|$ that provides a maximum in the gain margin curve slightly moves towards higher $|K_D|$ as higher $|K_P|$ are considered. For a $K_P \approx -0.25$, particularly, this occurs for

$K_D = -0.005$. A comparison between the evolution of gain and phase margin curves with K_P without and after considering integral and derivative gains as well is presented in Figure 3-10. Since the gain margin will be the most restricting factor and is slightly reduced for higher values of $|K_I|$, $K_I = -1$ is taken in order to be on the safe side.

Consequently, the maximum acceptable value for the proportional gain while complying with both gain and phase margin requirements is $K_P = -0.25$ provided that $K_D = -0.005$, which may be taken as definitive values, leaving only the final integral gain to be selected. On account of virtually all the considered integral gain values complying with the established stability requirements, another requirement is needed. If the values of settling time and overshoot are extracted from the pitch angle time responses for different values of the integral gain, as presented in Figure 3-11 a and Figure 3-11 b respectively, it can be clearly seen that both parameters have opposite tendencies, with the settling time decreasing and the overshoot increasing for higher $|K_I|$ values.

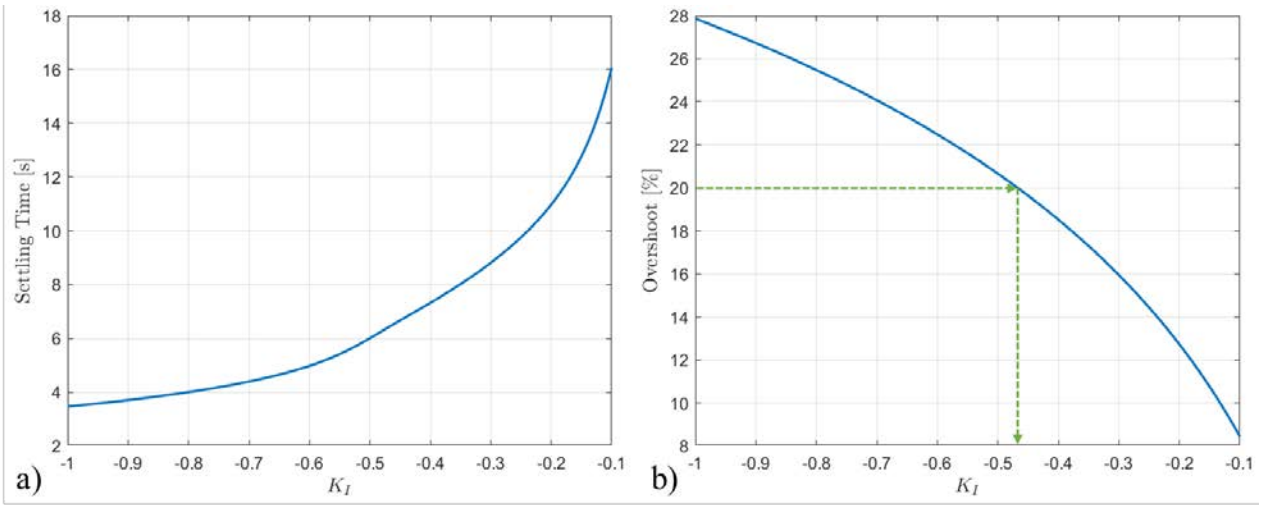

Figure 3-11: Evolution with K_I of the morphing UAV response's a) settling time and b) overshoot

Though lower settling times are desired, however, according to Ref. [25], an overshoot lower than 20% of the stationary value is mandatory for a control system to be considered as adequate. Therefore, if an overshoot of 20% is taken as the restricting factor, the maximum acceptable value for K_I is $K_I = -0.46$. An overview of the new gains for the flight control system of the modified configuration is presented in Table 3-2 below.

Table 3-2 Overview of the flight control system gains obtained for the morphing modified configuration

	K_α	K_q	K_P	K_I	K_D
Base Configuration	-1.375	-0.05	-0.15	-0.18	-0.004
Modified Configuration	-1.375	-0.06	-0.25	-0.46	-0.005

Finally, a comparison between the pitch angle time response of the modified configuration with the new flight control system gains (see Figure 3-12 b) and the ones from the base configuration (see Figure 3-12 a) is presented.

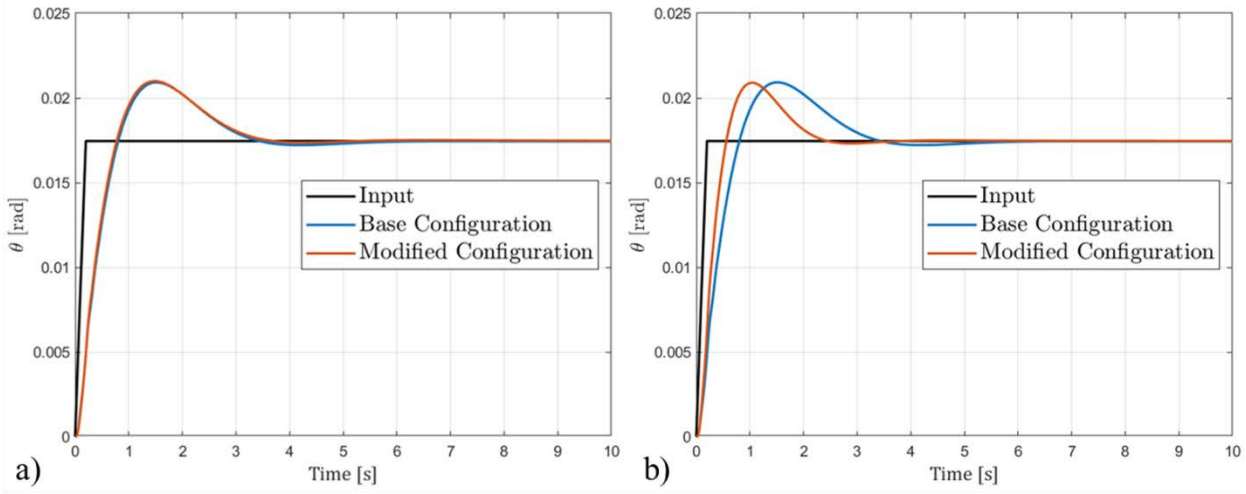

Figure 3-12: Comparison between the pitch angle time response of the base and modified configurations using a) the same gains and b) newly obtained gains for the modified configuration

4.0 CONCLUSIONS

The longitudinal stability of the bioinspired morphing UAV has been studied for its modified configuration in comparison to that of its base configuration. On account of the drone's geometrical features and its inherent static instability, a flight control system composed of an integrated PID-based pitch angle autopilot and an angle of attack and pitch rate stability augmentation system was designed in a previous work for the base configuration to provide an adequate response against an elevator deflection perturbation.

In the present work, said flight control system has been completely redesigned to account for the increased static stability of the modified morphing configuration, which is obtained by means of applying 1500V as input to a piezoceramic Macro Fiber Composite (MFC) actuator located over the wing's intrados, given that when using the same flight control system gains of the base configuration for the modified configuration, no tangible benefit is acquired. A strict minimum gain and phase margin requirements of 6 dB and 45° have been considered to conduct the redesign of the flight control system, together with a maximum overshoot of 20% of the stationary value allowed.

On account of the iterative nature of the flight control system design process, two full iterations have been conducted to select the most optimal gains, where a sweep of each gain was carried out to assess the restricting criteria, and provisional values were chosen to pass on to the next gains and continue the iterative process. It has been demonstrated how the slight stability improvement of the modified configuration can indeed lead to significant enhancements of the pitch angle time response provided the PID gains are optimized for said configuration.

REFERENCES

[1] A,Y,N, Sofla, S,A, Meguid, K,T, Tan, W,K, Yeo ''Shape morphing of aircraft wing: Status and Challenges''. Materiald and Design, 2010.

[2] Feng, N., Liu, L., Liu, Y., and Leng, J., "A bio-inspired, active morphing skin for camber morphing structures", *Smart Materials and Structures*, vol. 24, 2015, p. 035023.

[3] Moschetta, J. M., "The aerodynamics of micro air vehicle: technical challenges and scientific issues", *International Journal of Engineering Systems Modelling and Simulation*, Vol. 6, 2014, pp. 134-148.

[4] Marek, P. L., "Design, optimization and flight testing of a micro air vehicle" Ph.D. Dissertation, University of Glasgow, 2008.

[5] Flake, J., Frischknecht, B., Hansen, S., Knoebel, N., Ostler, J., &Tuley, B., "Development of the Stableyes Unmanned Air Vehicle", *8th International Micro Air Vehicle Competition*, 2004, pp. 1-10.

[6] Min, Z., Kien, V. K., and Richard, L. J. Y., "Aircraft morphing wing concepts with radical geometry change", *The IES Journal Part A: Civil & Structural Engineering*, vol. 3, 2010, pp. 188–195.

[7] Abdulrahim, M., and Lind, R. "Flight testing and response characteristics of a morphing gull-wing morphing aircraft", *AIAA guidance, navigation and control conference and exhibit*, 2004.

[8] Abdulrahim, M ''Flight dynamics and control of an aircraft with segmented control surfaces'', 2003.

[9] Bourdin, P., Gatto, A., and Friswell, M., "The application of variable cant angle winglets for morphing aircraft control," *24th AIAA Applied Aerodynamics Conference*, 2006.

[10] D. Dwarakanathan, R. Ramkumar, S. Raja and P. Siva Subba Rao ''Design, development and ground testing of hingeless elevons for MAV using piezoelectric composite actuators''. 2015.

[11] Fonterose, P. L., and Hall, C. E., "Development and flight testing of quantitative feedback theory pitch rate stability augmentation system", *Journal of Guidance, Control, and Dynamics*, vol. 19, 1996, pp. 1109–1115.

[12] Valavanis, K. P., "Principles of Guidance, Navigation, and Control of UAVs", *Handbook of Unmanned Aerial Vehicles*, Dordrecht: Springer, 2015.

[13] Szabolcsi, R., "Optimal PID controller-based autopilot design and system modelling for small unmanned aerial vehicle", *Review of the Air Force Academy*, vol. 16, 2018, pp. 43–58.

[14] Beygi, N., Beigy, M., and Siahi, M., "Design of fuzzy self-tuning PID controller for Pitch Control System of aircraft autopilot," *arXiv.org* Available: https://arxiv.org/abs/1510.02588v1.

[15] Chen, X.-H., Haq, E. U., and Lin, J., "Design, modeling and tuning of modified PID controller for autopilot in MAVs," *2016 17th IEEE/ACIS International Conference on Software Engineering, Artificial Intelligence, Networking and Parallel/Distributed Computing (SNPD)*, 2016.

[16] Fiuzy, M., Haddadnia, J., and Mousavi Mashhadi, S. K., "Designing an optimal PID controller for control the plans height, based on control of autopilot by using evolutionary algorithms," *Journal of Mathematics and Computer Science*, vol. 06, 2013, pp. 260–271.

[17] Bodson, M., "Reconfigurable nonlinear autopilot," *Journal of Guidance, Control, and Dynamics*, vol. 26, 2003, pp. 719–727.

[18] Shima, T., Idan, M., and Golan, O. M., "Sliding-mode control for Integrated Missile Autopilot guidance," *Journal of Guidance, Control, and Dynamics*, vol. 29, 2006, pp. 250–260.

[19] Jisha Shaji, and Aswin R B, "Pitch control of flight system using dynamic inversion and PID controller," *International Journal of Engineering Research and*, vol. V4, 2015.

[20] Ponrani, M. A., and Godweena, A. K., "Aircraft Pitch Control using PID Controller," *2021 International Conference on System, Computation, Automation and Networking (ICSCAN)*, 2021.

[21] Akbulut, A., and Adiguzel, T., "A comparative study of tuning of a PID controller using simulated annealing for a pitch attitude control system," *International Conference on Advances in Computing, Control and Networking - ACCN 2015*, 2015.

[22] Åström, K. J., and Hägglund, T., *PID controllers: Theory, design, and tuning*, Research Triangle Park, NC: ISA,1995.

[23] Golnaraghi, M. F., and Kuo, B. C., *Automatic Control Systems*, New York: McGraw-Hill Education, 2017.

[24] Nelson, R. C., *Flight stability and automatic control*, Chennai: McGraw-Hill Education (India) Private Limited, 2010.

[25] Cook, M., *Flight dynamic principles: A Linear Systems Approach to aircraft stability and control*, Amsterdam etc: Elsevier, 2007.

[26] Barcala-Montejano, M., Rodríguez-Sevillano, A. Bardera-Mora, R., García-Ramirez, J., de Nova-Trigueros, J., Urcelay-Oca, I., and Morillas-Castellano, I., "Smart materials applied in a micro remotely piloted aircraft system with morphing wing", *Journal of Intelligent Material Systems and Structures,* vol. 29, 2018, pp. 3317-3332.

[27] M. Barcala-Montejano, A. Rodríguez-Sevillano, J. Crespo-Moreno, R. Bardera-Mora y A. Silva-González, «Optimized performance of a morphing micro air vehicle» de *International Conference on Unmanned Aircraft Systems (ICUAS)*, Denver, CO, 2015.